Miniaturised MultiMEMS sensor development

Mathieu Hautefeuille[1)], Brendan O'Flynn[2)], Frank Peters[1,3)], Conor O'Mahony[2)]
[1)] Centre for Telecommunication Value-Chain Research, Tyndall National Institute, Lee Maltings, Cork, Ireland
[2)] Tyndall National Institute, Lee Maltings, Cork, Ireland
[3)] Department of Physics, University College, Cork, Ireland

***Abstract**: This paper describes the design, fabrication and initial characterisation of a MEMS-based environmental monitoring system. Intended for use with miniaturised Wireless Sensor Network (WSN) motes, the die measures 3 x 3mm and incorporates humidity, temperature, corrosion, gas and gas flow velocity sensors on a single substrate. Fabricated using a combination of surface and bulk micromachining technologies, the sensor system is designed to replace discrete components on WSN module boards, thereby minimising space consumption and enabling smaller, cheaper wireless motes. Sensors have been characterised over a wide range of environmental conditions. An analysis of the effects of changes in environmental parameters other than the measurand of interest on the performance of the temperature and humidity sensors has been carried out, and corrections applied where necessary. A variety of corrosion monitors have been demonstrated. A gas flow velocity sensor, based on forced convective heat transfer and which has been thermally isolated from the silicon substrate in order to reduce power consumption and improve sensitivity at low flow-rates, has also been presented. The paper also outlines the design of the next generation sensing platform using the novel 10mm wireless cube developed at Tyndall.*

1. INTRODUCTION

The coming years will see the emergence and deployment of low cost, low power, intelligent wireless sensor networks (WSN) in various applications such as environmental monitoring, agriculture, traffic control, home automation and healthcare [1]. Miniaturisation and modularity of the sensing platforms will be necessary for these and many other uses that require large numbers of dispersed monitoring points.

The Tyndall National Institute is developing miniaturised 'motes' that incorporate customisable sensor interface boards for use in highly modular wireless platforms. The interface boards exist in both 25mm×25mm and 10mm×10mm form factors and allow a combination of different sensors to be connected to computational and RF components [2], [3]. Depending on the target application of the sensing platform, the list of possible configurations to consider must be carefully studied, and in order to allow further progress along the roadmap towards

smaller, cheaper, multifunctional motes, miniaturisation of the sensors and conditioning circuitry is essential [4]. Since discrete sensors are bulky, expensive and consume valuable board area, the use of MEMS-based integrated sensors will allow further reduction of the platform size.

This paper describes progress towards a multifunctional sensor for wireless sensor network platforms. Fabricated using a combination of surface and bulk micromachining technologies, the CMOS-compatible sensor incorporates temperature, humidity, corrosion, gas and gas flow velocity monitors.

2. MULTI-MEMS DESIGN AND FABRICATION PROCESS

The fabrication process flow presented in figure 1 is compatible with CMOS technology, as the bottom metal electrode of the MEMS process doubles as the CMOS top metal layer. It enables the development of five different environmental sensors: temperature, corrosion, humidity, gas, and gas flow velocity, figure 1. The fabrication of a monolithic MEMS+CMOS sensor die, as well as preliminary sensor characterisation work, has already been described in [5].

The substrate material is single-crystal silicon. The first steps of the process flow involve the deposition and patterning of a thin metal layer (0.5µm Al/1%Si) over an oxide film. This is the active sensing layer for temperature, corrosion and gas flow sensors, and acts as the bottom electrode of the humidity sensor. A passivation oxide is then deposited and selectively removed over corrosion, gas and humidity sensors (figure 1(a)). The third step consists of a polyimide deposition (figure 1(b)). This polymer layer acts as porous dielectric for the humidity sensor and a sacrificial layer for the gas sensor element (a fixed-fixed beam). A second metallic layer (1.0 µm Al) is then deposited, forming the top electrode of the humidity sensor and active element of the gas sensor, (figure 1(c)). The silicon substrate is then etched from beneath the gas flow velocity sensor in order to obtain good thermal isolation and improved sensitivity (figure 1(d)). Finally, the polyimide sacrificial layer is selectively removed (figure 1(e)).

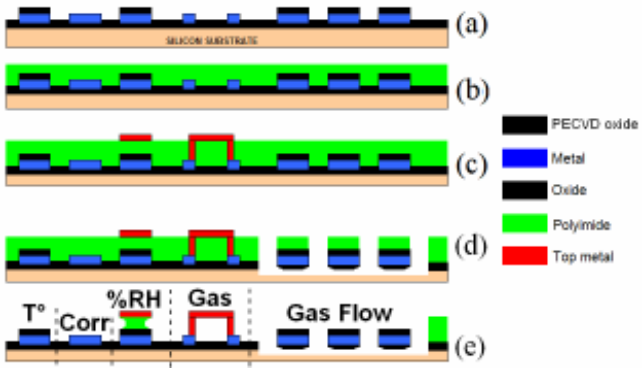

Figure 1: Multisensor fabrication process.
From left to right: temperature sensor, corrosion sensor, humidity sensor, gas sensor, gas flow velocity sensor.

3. MULTIPLE MEMS DEVELOPMENT AND TEST

3.1 Experimental details

A test setup has been developed in order to process, record and analyse data from all sensors over a period of time. Figure 2 shows a schematic of the MEMS bare die which have been wirebonded in dual-in-line (DIL) packages for testing. They incorporate three different types of sensors: temperature, humidity and corrosion; it was not possible to characterise the

gas sensors with the current experimental setup. Instead, preliminary results have been described in [5]. A range of corrosion structures have been tested, consisting of ladders [6], electrolytic migration detectors [7], and triple track comb patterns [8].

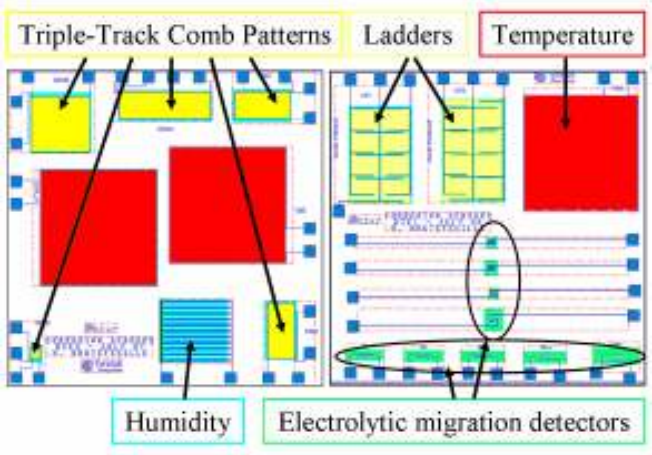

Figure 2: Test structures with multiple MEMS sensors.

The sensitivity, stability, and hysteresis of each sensor can be affected by changes in parameters other than the measurand of interest. It is important to investigate the isolation of the sensors from these parameters over a wide range of environmental conditions. For the tests described in the following sections, the die have been tested in a TAS HTCL225 climatic chamber [9]. Humidity and temperature inside the chamber are measured using calibrated sensors. Sensor resistance values have been measured using Keithley 2430 and Agilent 34411A multimeters, and capacitance measurements were read on an Agilent 4284A LCR meter with a bias of 50mV at a frequency of 100 kHz. The substrates of the die were grounded to avoid parasitic charges, while the output data was both saved and displayed using an Agilent VEE software program.

3.2 Effect of humidity on temperature sensor performance

The temperature sensor presented here is a 0.5µm x 2µm x 2mm meander of Al-1%Si. The resistance R of this metal track varies with temperature T according to

$$R(T) = R_0\left(1 + \alpha\left[T - T_0\right]\right), \quad (1),$$

where R_0 is the sensor resistance at a known temperature T_0, and α is the thermal coefficient of resistance (TCR) of the material. However, other parameters such as the ambient gas composition and its relative humidity can affect the performance of temperature sensors, and they have to be incorporated to correct the final sensor response.

3.2.1 Effect of humidity on sensor sensitivity and hysteresis

The effect of humidity on the temperature sensor performance given in (1) remains relatively insignificant over a wide range of humidity from 20%RH to 90%RH, and the hysteresis is negligible.

3.2.2 Humidity isolation of the temperature sensor

The die were placed in the chamber at constant temperature, while humidity was ramped up and down from 20%RH to 90%RH. The response of the sensor gives temperature according to (1), and it can be compared to the actual temperature inside the chamber. The error (defined as the difference between the chamber temperature and the sensor response according to (1)) is then calculated and is not negligible, showing a dependence on humidity of the sensor. A similar structure without passivation layer has been equally affected by humidity, suggesting that the passivation layer passivation does not prevent

errors caused by humidity variations. A model of the error is then constructed for each temperature value. Figure 3 gives an example of sensor error and such a model at a fixed temperature of 25°C.

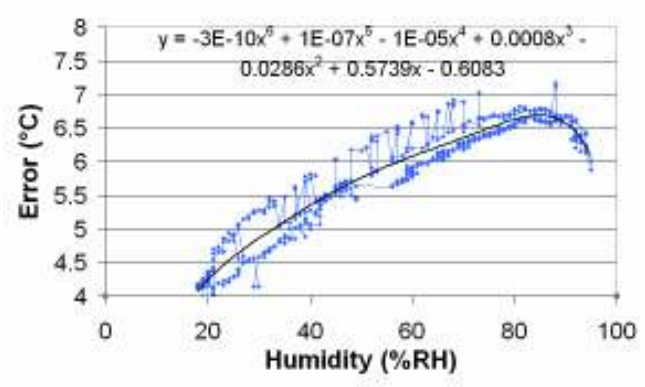

Figure 3: Humidity dependence of temperature sensor at 25°C.

The error can be corrected using the model in order to correlate temperature and humidity effects. The actual temperature, obtained after correction for humidity effects, is given by:

$$T = T_{meas} - corr \qquad (2),$$

where the typical correction for the effects of humidity on the temperature sensor performance is

$$corr = 3.10^{-10} RH^6 + 10^{-7} RH^5 - 10^{-5} RH^4 + 8.10^{-4} RH^3 - 0.03RH^2 + 0.57RH - 0.61 \qquad (3)$$

We can see on figure 4a that the correction reduces the average error from as high as 30% to a more acceptable maximum value of 7%. An example of the corrected sensor characterisation taking humidity into account is presented on figure 4b. It shows that the sensor output is closer to the true temperature value after treatment.

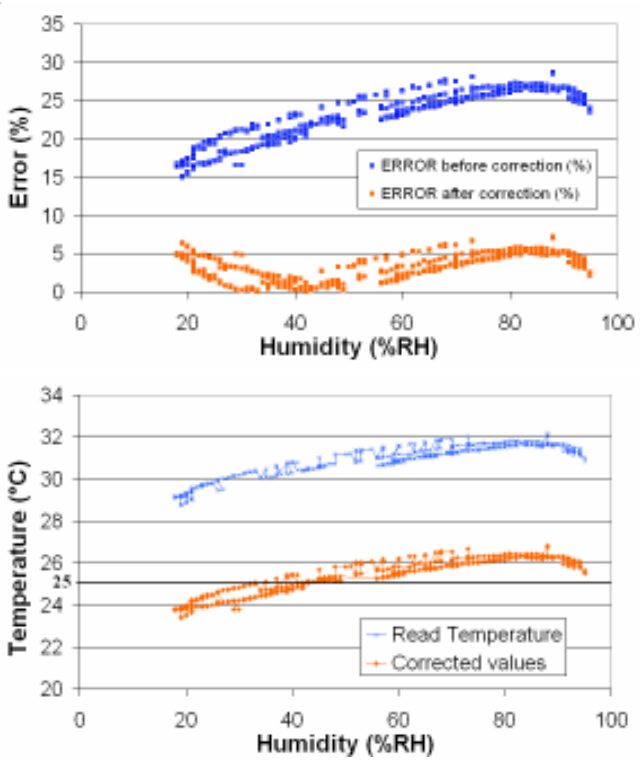

Figure 4: (a) Correction of the humidity induced error; (b) Temperature after correction - measurements at 25°C.

3.3 Temperature effects on humidity sensors

The capacitive humidity sensors fabricated at Tyndall are based on two metal electrodes of common area A, separated by a porous polyimide layer of thickness d [5]. The dielectric constant ε_r of the polymer is a function of humidity, and the typical response of the sensor is given by:

$$C(\%RH) = \frac{\varepsilon_0 \varepsilon_r (\%RH) A}{d} \qquad (4)$$

3.3.1 Temperature effects on hysteresis

It has already been demonstrated that use of polyimide as the active sensing layer will lead to a hysteresis effect, as its water absorption and desorption rates are different [10]. However, temperature changes will not amplify this effect. This

simplifies the compensation model of temperature effects on the humidity sensor [11].

3.3.2 Temperature effects on sensitivity

It has already been proven that temperature affects the sensitivity of capacitive humidity sensors, and that these effects can be compensated [11]. In order to correct the sensor response, the data obtained from the humidity sensor during the tests described in [5] was used to calculate its sensitivity for different fixed temperatures, when humidity is ramped up and down. Figure 5 shows the evolution of the capacitance response for different temperatures from 10°C to 70°C.

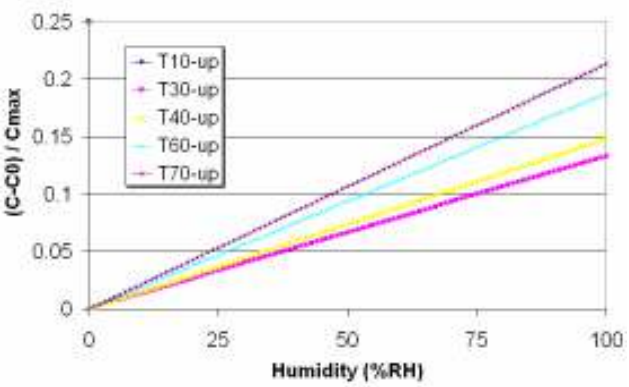

Figure 5: Humidity sensor response at various temperatures.

The sensor sensitivity (d*C*/d(%RH) can be calculated and plotted against temperature, as shown on figure 6 for four sensors of the type described in [5]. It is clear that temperature has an effect on the sensitivity, as a difference of 25fF per %RH is attained between 20°C and 70°C [5]. The variations from one die to another are explained by fabrication tolerance, as polyimide thicknesses can vary slightly across the wafer.

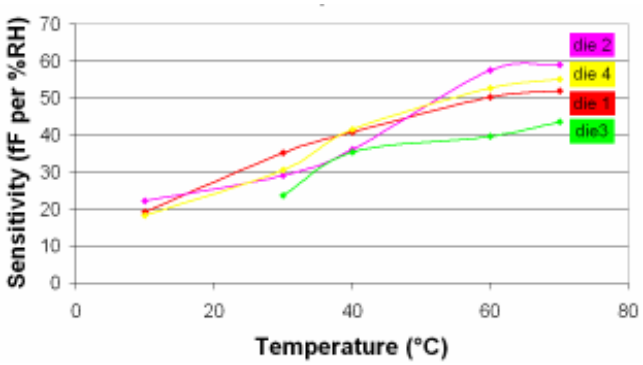

Figure 6: Sensitivity of humidity sensors as a function of temperature.

A model of the sensitivity against temperature can then be constructed, and the fitted curves are third order equations. The temperature compensation equation for the sensor presented in figure 6 for die 2 is given by:

$$S = -0.0003T^3 + 0.047T^2 - 1.448T + 30.134 \quad (5)$$

3.3.3 Temperature isolation of the humidity sensor

The temperature isolation of the humidity sensor is not perfect as the sensor response is temporarily modified during temperature transitions at a fixed humidity.

If the application of this multiple sensing platform requires a fast accurate response, a correction will be necessary. However, for typical applications in environmental monitoring which do not demand to follow fast changes, this type of compensation is not critical, as the sensor response corrects itself within a few minutes.

3.3.4 Multiple measurements and compensation

By combining the temperature obtained from equation (2) with equation (5), it is possible to give ΔRH as a function of the measured capacitance C and the measured resistance R.

3.4 Corrosion sensors

The ambient conditions inside our climatic chamber are not particularly corrosive as there is no gas other than air present, and no salts that could accelerate corrosion of the structures. Therefore, accelerated tests such as the ones described in [6] and [12] were required to characterise the sensors.

Subsequently, combinations of triple-track comb patterns [13] and ladder [14] corrosion monitors were characterised as a function of temperature and humidity. For the triple-track structures, the middle resistor was grounded, while the structures on each side were inversely biased. As the middle line corrodes, its resistance gradually increases, until it is fully corroded and becomes an open circuit. This type of device can monitor corrosion kinetics and corrosion rate variations. Ladder-type monitors demonstrate an incremental increase of the middle line resistance as electrolytic corrosion occurs. The incremental corrosion depends on the different gaps between the ladder rungs.

Examples of corrosion data are shown in figure 7 for two triple-track comb pattern structures, and in figure 8 for the middle line of a typical ladder.

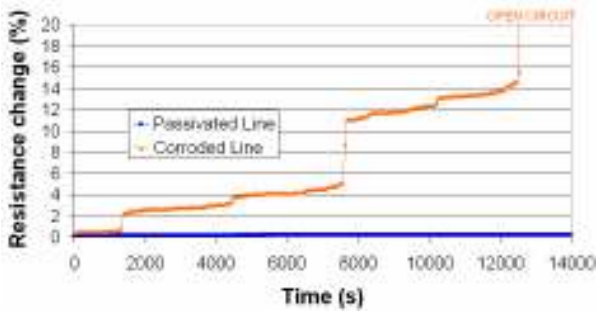

Figure 7: Resistance monitoring of a triple-track corrosion sensor and a passivated line at 60°C, 70%RH, 3V bias.

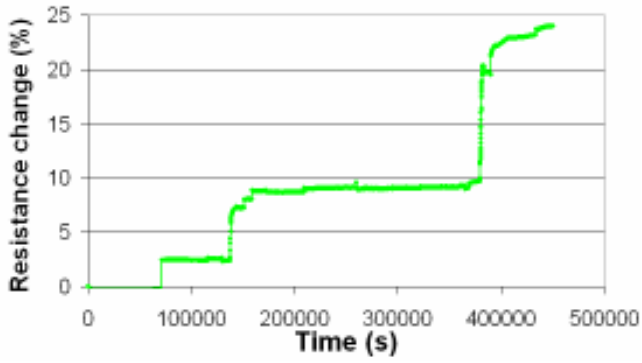

Figure 8: Resistance monitoring of the middle line of a ladder at 60°C, 70%RH, 5V bias.

As can be seen on figure 7, the corroded structure reacts in an incremental step fashion until the line is fully corroded and becomes an open circuit. The passivated metal line is used as a control and shows no resistance increase. Figure 8 shows the incremental response of a ladder sensor. Two different voltage biases have been used here under fixed ambient conditions. A change of 25% in the line resistance is obtained after 125 hours. We expect extensive tests in more corrosive environments to show that corrosion rates can be better investigated with the ladder structure.

3.5 Gas flow sensor

Flow velocity is a key target parameter in fields ranging from fluidics applications such as vacuum leakage and flow detection to automotive and medical industries. The range of flows to measure can be very broad, and its lower limit reaches a few nl/min, requiring miniaturised sensing structures.

Thermal flow sensors seem to offer the best method of measuring low flow rates [15]. Consisting of thermally isolated microstructures, these operate by measuring variations in the structure's thermal properties in response to changes in the surrounding

ambient. They can also be used in a variety of other sensing applications, such as infra-red detection, pressure monitoring, gas detection and accelerometers [16].

The design of these structures has been made possible with bulk micromachining: after deposition of the active metal meanders on an oxide table, 160µm deep trenches are isotropically etched into the silicon substrate, resulting in a series of thermally isolated resistive meanders, Figure 1(g). Figure 9 shows a detail of the substrate underetching and suspended metal meander.

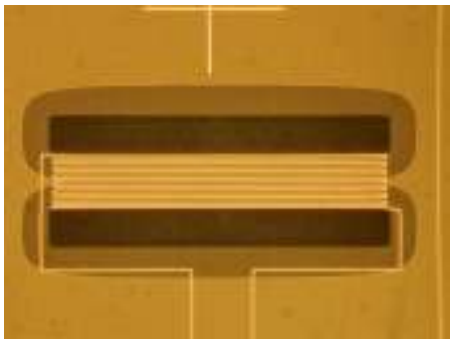

Figure 9: Microscope image of the active metal meander. The isotropic etch is visible.

The working principle of this sensor is based on the theory of forced convective heat transfer [17]. The sensor consists of three suspended structures: one resistive heater and two temperature sensors located upstream and downstream of the heater. The temperature profile across the sensors varies with flow rate and direction. This gas flow sensor design offers excellent thermal isolation of the heating and sensing metal meanders, allowing lower power consumption of the heater (figure 10), and good sensitivity (figure 11).

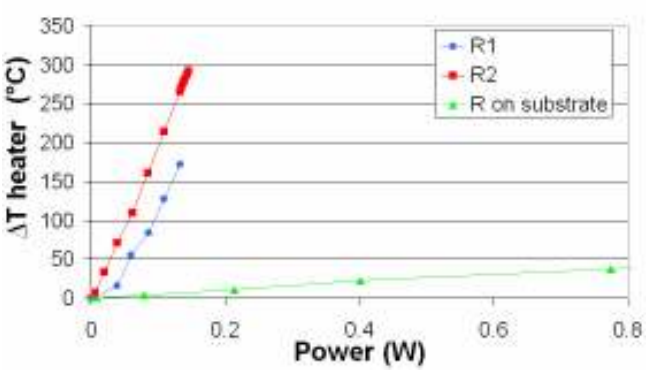

Figure 10: Heating of three structures as a function of applied electrical power: one meander on substrate and two suspended structures with different dimensions.
Note the reduction in power consumption of the suspended structures.

The preliminary experimental analysis of fabricated gas flow sensors performances has been conducted in ambient environment. Compressed air flowing on the surface of the structure through a controlled flow-meter is oil and moisture free by industrial standards. Temperature variations presented here are compared to a reference when no electrical power is applied across the heater. They are calculated from precise resistance measurements.

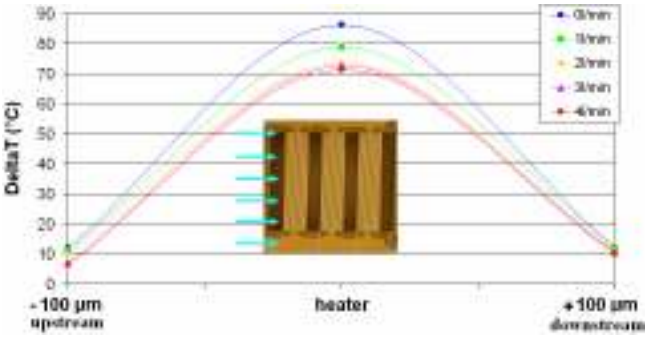

Figure 11: Preliminary results of flow sensor in open air (V_{in} = 2.5V).

Results show that symmetrical sensors on each side of the heater allow both flow detection and velocity measurements as depicted on figure 12 for V_{in}=2.5V. The sensor displays greatest sensitivity in the 2-3L/min range. The power consumption of the

structure ranges from 10mW at 1.5V to 50mW at 4V. A flow velocity experimental test rig is currently being constructed for precise testing.

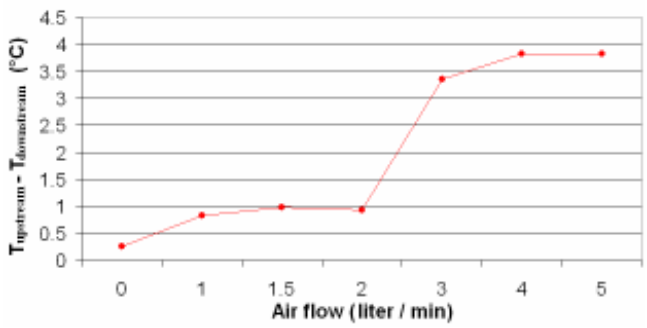

Figure 12: Temperature difference between upstream and downstream as a function of the flow velocity (V_{in}=2.5V).

3.5 Gas sensor

A process compatible gas sensor has also been fabricated and tested. It consists of a 100µm long suspended metal beam, with a cross-sectional area of 1µm x 5µm. Initial results have already been described in [5].

4. INTEGRATION AND DEPLOYMENT

As presented in [3] and [5], Tyndall has developed modular wireless platforms in different formats for deployment in WSN. The multi-sensor die can then be attached to these platforms as has already been demonstrated on a 25mm x 25mm PCB board [2].

On figure 13, the deployment of the present sensors on two Tyndall motes is depicted. The 10mm x 10mm version has been made possible thanks to the compatibility of the MEMS process with CMOS technology. Hence, signal conditioning circuitry has been designed on the sensor die, reducing the space taken by discreet components mounted at the back of the 25mm layer.

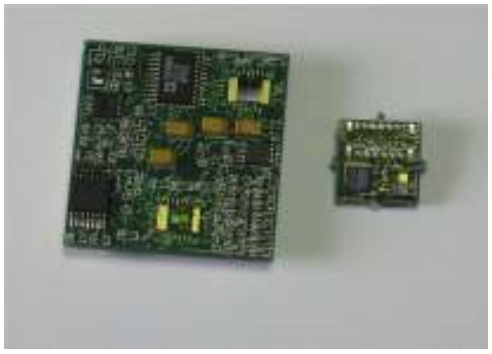

Figure 13: MEMS multi-sensor dies deployed on 25mm (left) and 10mm (right) wireless motes.

Integrating the multi-sensor die described in this paper with the wireless motes will allow deployment and testing in outdoor environments. This will be achieved in the following stages of the project, and will enable increased signal processing and cross-correlation between sensors.

5. CONCLUSION

The design, fabrication and test of multiple MEMS sensors on a single die have been presented in this paper. Cross-correlation between different sensors has been investigated in a controlled environment; models that correct the unwanted effects of temperature and humidity have been developed and validated. Future work will involve gas and gas flow velocity sensor characterisation and deployment of the complete wireless platform in the field.

ACKNOWLEDGEMENTS

The authors would like to acknowledge the Tyndall Central Fabrication Facility for processing of the devices. This work has been supported by Science Foundation Ireland under the CTVR network.

REFERENCES

[1] Culler, D., Estrin, D., Srivastava, M., "Overview of sensor networks", IEEE Computer, August 2004.

[2] S. Harte, B. O'Flynn, R.V. Martinez-Catala, E.M. Popovici, , "Design and Implementation of a Miniaturised, Low Power Wireless Sensor Node", *Proc. 18th European Conference on Circuit Theory and Design*, pp. 894-897, August 27-30 2007.

[3] J. Barton, G. Hynes, B. O'Flynn, K. Aherne, A. Norman, A. Morrissey, "25mm Sensor-Actuator Layer: A miniature, highly adaptable interface layer", *Sensors and Actuators A-Phys.,* Vol. 132, November 2006, pp. 362-369.

[4] http://www.vtt.fi/inf/pdf/tiedotteet/2007/T2381.pdf

[5] M. Hautefeuille, C. O'Mahony, B. O'Flynn, K. Khalfi, F. Peters, "A MEMS-based wireless multisensor module for environmental monitoring", *Journal of Microelectronics Reliability*, Vol. 48, No. 6, June 2008, pp. 906-910.

[6] N.L. Sbar, R.P. Kozakiewicz, "New Acceleration Factors for Temperature, Humidity, Bias Testing", *Proc. 16th Annual Reliability Physics Symposium*, pp. 161-178, 1978.

[7] S.K Fan, J.W. McPherson, "A Wafer-Level Corrosion Susceptibility Test for Multilayered Metallization", 26th Annual International Reliability Physics Symposium, pp. 50-57, 12-14 April, 1988.

[8] H.R. Shea, A. Gasparyan, H.B. Chan, S. Arney, R.E. Frahm, D. López, S. Jin, R.P. McConnell, "Effects of Electrical Leakage Currents on MEMS Reliability and Performance", *IEEE Transactions on Device and Materials Reliability,* Vol.4, No.2, June 2004.

[9] http://www.tasltd.co.uk/microspec.html

[10] C. Laville, C. Pellet, "Interdigitated Humidity Sensors for a Portable Clinical Microsystem", IEEE Transactions on Biomedical Engineering, vol.49, no.10, pp. 1162-1167, October 2002.

[11] C.Y. Lee, G.B. Lee, "Micromachine-based humidity sensors with integrated temperature sensors for signal drift compensation", *Journal of Micromechanical Microengineering*, Vol.13, pp.620–627, 2003.

[12] J.N. Sweet, M.R. Tuck, D.W. Peterson, D.W. Palmer, "Short and long loop manufacturing feedback using a multi-sensor assembly test chip", *IEEE Transactions on Components, Hybrids, and Manufacturing Technology*, Vol.14, No.3, September 1991.

[13] P.R. Troyk, R. Frankovic, J.E. Anderson, "Experimental Techniques for Electrical Testing of Microelectronics Coating", IEEE Transactions on Components, Hybrids and Manufacturing Technology, vol. 14, no. 2, pp. 428-435, June 1991.

[14] J.N. Sweet, "The Use of Speciql Purpose Assembly Test Chips for Evaluating Reliability in Packaged Devices", International Workshop on Wafer Level Reliability, Final Report, pp. 77-82, 25-28 October 1992.

[15] M. Aschauer, H. Glosch, F. Hedrich, N. Hey, H. Sandmaier, W. Lang, "Thermal flow sensors for liquid and gases based on combinations of two principles", *Sensors and Actuators*, A, 73(1-2):7-13, 1999.

[16] R.P. Manginell, J.H. Smith, A.J. Ricco, An overview of micromachined platforms for thermal sensing and gas detection, in: Proceedings of SPIE on International Society of Optical Engineering, 1997, pp. 273–284.

[17] M. Elwenspoek, Thermal Flow Microsensors, CAS99, (2):423-425, 1999.